Journal Name

ARTICLE TYPE

Cite this: DOI: 00.0000/xxxxxxxxxx

Topological signatures and stability of hexagonal close packing and Barlow stackings

Georg Osang,[a] Herbert Edelsbrunner,[a] and Mohammad Saadatfar[b] *

Received Date
Accepted Date

DOI: 00.0000/xxxxxxxxxx

[a] Institute of Science and Technology Austria, Am Campus 1, 3400 Klosterneuburg, Austria
[b] Department of Applied Mathematics, Research School of Physics and Engineering, The Australian National University, Canberra ACT, 2601, Australia

* mohammad.saadatfar@anu.edu.au

Two common representations of close packings of identical spheres consisting of hexagonal layers, called Barlow stackings, appear abundantly in minerals and metals. These motifs, however, occupy an identical portion of space and bear identical first-order topological signatures as measured by persistent homology. [Saadatfar *et al., Nat. Comm.*, 2017, **8**, 1–11]. Here we present a novel method based on k-fold covers that unambiguously distinguishes between these patterns. Moreover, our approach provides topological evidence that the FCC motif is the more stable of the two in the context of evolving experimental sphere packings during the transition from disordered to an ordered state. We conclude that our approach can be generalised to distinguish between various Barlow stackings manifested in minerals and metals.

1 Introduction

When identical hard spheres are packed together, they naturally form a disordered granular structure that fills 64% of the space. Although the packing structure is disordered, the limiting packing density of 64% is highly reproducible. This phenomenon was extensively studied by J. D. Bernal in the 1950s and 1960s and the limiting density of 64% is known as the Bernal density or φ_{Bernal}. Numerous experimental and numerical studies have extended Bernal's seminal findings and reported that a stable configuration of frictional mono-disperse spheres can exist at densities ranging from $\varphi = 0.55$ to $\varphi = 0.64$ [1–3]. It is possible to break through φ_{Bernal} by intensely vibrating [4] or cyclically shearing [5] of the packing structure. This forces the density of the packing to increase to the maximum of $\varphi \approx 74\%$, which is reserved for the FCC (face-centred-cubic) or HCP (hexagonal-close-packing) crystalline structures. Beyond Bernal's density, φ_{Bernal}, crystalline clusters inevitably appear in highly mono-disperse sphere packings. An obvious question to ask is: How are the spheres packed together locally in the disordered regime and what happens to these local structures during the transition through φ_{Bernal} all the way to $\varphi_{max} = 74\%$ of FCC or HCP. A thorough understanding of the crystallisation process in such systems crucially relies on finding key sphere scale patterns in the amorphous states and their evolution while the packing density increases to $\approx 74\%$.

The topological and analytical paradigms presented in this paper provide a new approach to understanding the accessible regions of the configurational landscape of granular matter. Using the new approach, we study experimental and numerical packings of hard-sphere granular materials. Our experiments harness X-ray computed tomography, three-dimensional image analysis, and numerical simulations to accurately access the 3D structure of the sphere packings. Recent studies have analysed sphere packings using persistent homology ("persistence"), and shown that FCC and HCP motifs have identical persistence diagrams when only considering the union of balls around the sphere center points [4]. However, it is critically important to distinguish the topological signatures of FCC and HCP in order to understand structural and topological evolution of granular packings during disorder-order transition that could lead to the prevalence of FCC or HCP patterns.

This paper aims to address the shortcomings of persistent homology of the union of balls by introducing persistent homology of the k-fold cover, or k-cover persistence for short. We show that k-cover persistence can successfully characterise the crystallisation process of our experimental granular packings and, further, unambiguously distinguish between FCC and HCP patterns. Our results open new perspectives to describe the grain-scale ordering of granular structure while grains re-arrange to increase their

structural density. We show, for the first time, that with k-cover persistence already for $k = 4$, FCC and HCP show distinct features in their k-cover persistence diagrams as seen in Figure 4.

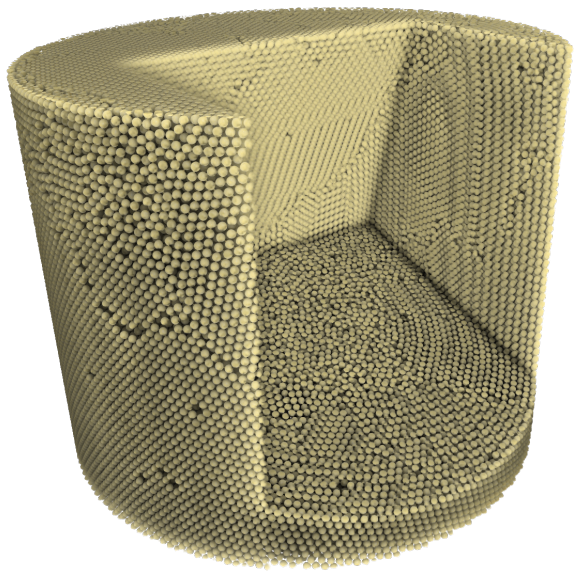

Fig. 1 3D rendering of the experimental packing. A cut-out section shows the bulk crystallisation and partially crystallised regions

2 Persistent homology of multi-covers

Persistent homology [6–8] has been used to analyze sphere packings before. [4] In this setting, persistence is applied to a discrete point set X, such as the set of sphere centers of a packing. Ordinarily, the union of balls of some variable radius r around these points is considered, and how the topology of this union of balls changes as r increases from 0 to infinity. Persistent homology tracks these topological changes, i.e. the emergence (births) and disappearance (deaths) of topological features. In the 3-dimensional setting, these topological features are *connected components* (or the *gaps* between them), *closed loops* (or the *tunnels* they form), and *closed surfaces* (or the hollow *voids* they surround). The output is a *persistence diagram* $\mathrm{Dgm}(f)$, capturing the "life" of each topological feature, represented by a point in 2D with the x-coordinate being the time (or more precisely radius) of birth (i.e. when the feature emerges), and the y-coordinate being the time of death (i.e. when the feature disappears). The persistence diagram is invariant under isometries (rotations, translations, reflections) of the discrete point set. Furthermore, it has an important stability property: Small perturbations in the original point set cannot lead to large changes in the persistence diagram. [9]

Here we generalize this notion of persistence of a discrete point set to what we call *persistence of the k-fold* cover (or *k-cover persistence* for short) [10]. In this formalism, instead of the union of balls, we consider the k-fold cover, which is the subset of $\mathbb{R}^3$ where at least k balls overlap. (The k-fold covers can also be viewed as sublevel sets of the k-th distance function, f_k, measuring the distance of a point in $\mathbb{R}^3$ to its k-th closest point in X.) The previously described case for the union of balls is the special case for $k = 1$. Just like the union of balls, the k-fold cover grows as we increase the radius of the balls, and its topology changes; see Figure 2 for an example with $k = 3$. The computed persistence diagram, $\mathrm{Dgm}(f_3)$, of the point set X is shown in Figure 3, showing the birth and death times of various topological features in the 3-fold cover. In general, we denote the k-cover persistence diagram of a point set as $\mathrm{Dgm}(f_k)$.

3 Characterisation of FCC and HCP patterns

In order to understand the persistence diagrams of our experimental datasets, we first have to analyze how geometric structures in FCC and HCP packings yield points in $\mathrm{Dgm}(f_4)$. In particular we need to understand tetrahedral and octahedral cavities and their adjacency relations. The first and last rows of Figure 5 show schematic sketches of the FCC and HCP packings respectively. In our analysis, we will focus on $\mathrm{Dgm}_0(f_4)$, the persistence diagram restricted to 0-dimensional topological features (i.e. connected components), as they are easier to interpret geometrically than the higher-dimensional features.

Assuming spheres of diameter 1, a component of the 4-fold cover emerges at the center of a tetrahedral cavity at radius $\sqrt{6}/4$. Within an octahedron, the 4-fold cover emerges at radius $\sqrt{2}/2$ at its center. (Both of these radii correspond to the circumradii of the tetrahedra and octahedra.) The radius for when these components merge with other components depends on a slightly larger neighbourhood. If two tetrahedra are face-adjacent, a configuration only present in HCP, the components merge earlier than if they are only edge-adjacent (as present in both FCC and HCP, but with different multiplicities). A more detailed geometric analysis is provided in the supplemental material.

Figure 2 can provide some intuition if equilateral triangles are used as an intuitive proxy for tetrahedra, and the square as proxy for an octahedron.

Table 1 summarizes the features we see in $\mathrm{Dgm}_0(f_4)$ of the FCC and HCP packings. While zero-persistence features are usually not considered as features, we include the one stemming from octahedra for completeness as they will become non-zero persistence features once these octahedra get deformed, e.g. in Figures 5, 6 and 8.

Table 1 Summary of features in $\mathrm{Dgm}_0(f_4)$ for FCC and HCP packings. Note that face-adjacent tetrahedra are only present in HCP packings, but not in FCC packings

Point in $\mathrm{Dgm}_0(f_4)$	Decimal	Feature
$(\sqrt{6}/4, \sqrt{6}/3)$	(0.61, 0.82)	**A** two face-adjacent tetrahedra
$(\sqrt{6}/4, \sqrt{3}/2)$	(0.61, 0.87)	**B** two edge-adjacent tetrahedra
$(\sqrt{2}/2, \sqrt{3}/2)$	(0.71, 0.87)	**C** octahedron-tetrahedron adjacency
$(\sqrt{2}/2, \sqrt{2}/2)$	(0.71, 0.71)	**D** octahedron (zero-persistence)

Deformations. We furthermore investigate the changes in $\mathrm{Dgm}_0(f_4)$ as an FCC packing is deformed into an HCP packing by moving a layer of spheres over a saddle point, see Figure 5 for the resulting $\mathrm{Dgm}_0(f_4)$. Note that when a packing is continuously

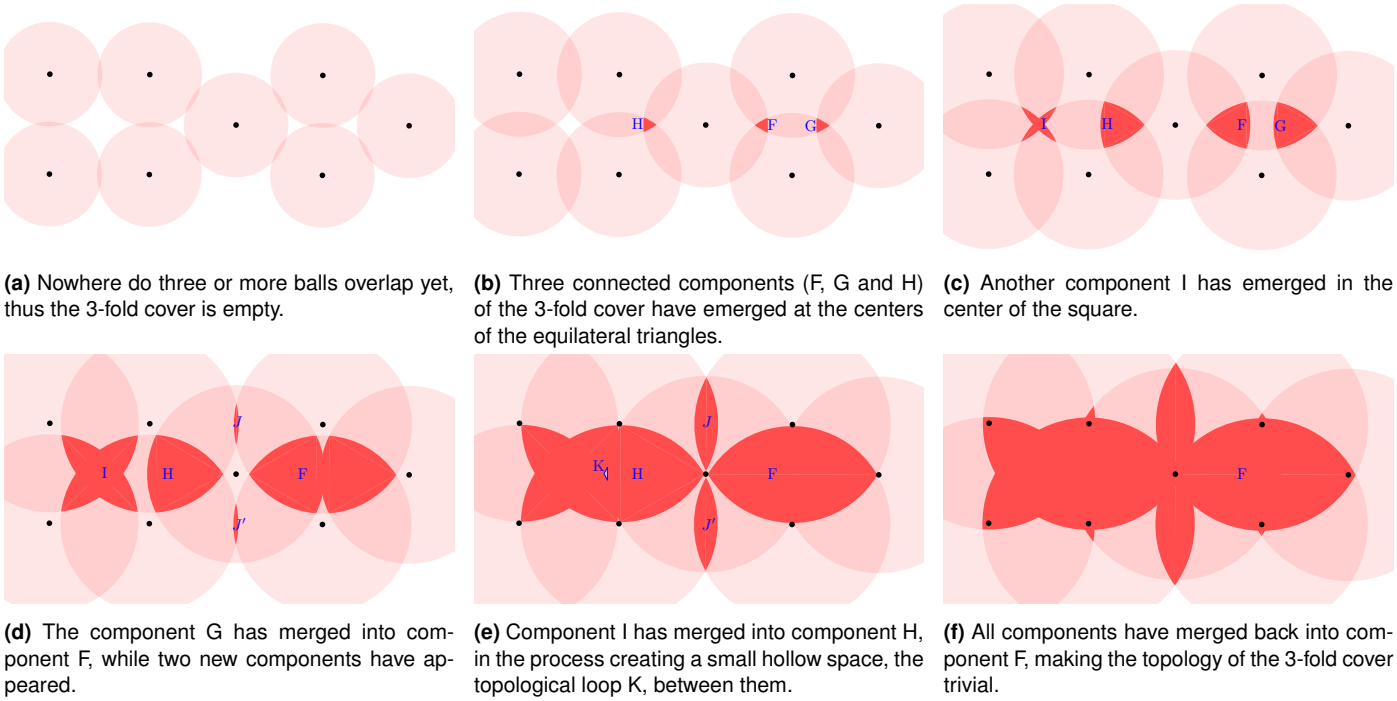

(a) Nowhere do three or more balls overlap yet, thus the 3-fold cover is empty.

(b) Three connected components (F, G and H) of the 3-fold cover have emerged at the centers of the equilateral triangles.

(c) Another component I has emerged in the center of the square.

(d) The component G has merged into component F, while two new components have appeared.

(e) Component I has merged into component H, in the process creating a small hollow space, the topological loop K, between them.

(f) All components have merged back into component F, making the topology of the 3-fold cover trivial.

Fig. 2 Development of the 3-fold cover for increasing radii, with the birth and death of topological features (components, loops). For each point, the ball of radius r is drawn in semi-transparent pink. The 3-fold cover is where at least three of these balls overlap, and is drawn in solid red.

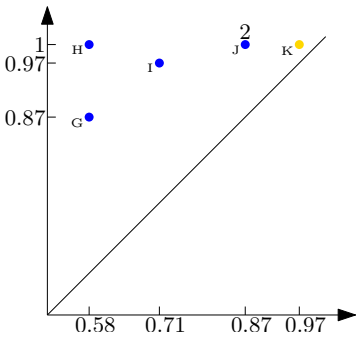

Fig. 3 3-cover persistence diagram of the example point set from Figure 2, representing the topological changes over time. Each point is annotated with the label of the topological feature present in Figure 2. Features J and J' have the same times of birth and death, and are represented by point J which thus has multiplicity 2. Feature F is not present as its time of death is at infinity.

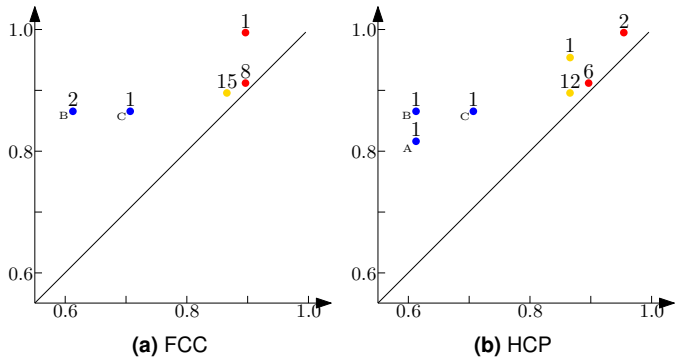

Fig. 4 4-cover persistence diagrams of FCC and HCP packings. 0-dimensional topological features (components) are shown in blue, 1-dimensional features (loops) in yellow, 2-dimensional ones (voids) in red. Each persistence point is annotated above with a relative multiplicity, indicating how many topological features with the given birth and death coordinate exist per sphere. Furthermore each 0-dimensional persistence point is annotated (in brackets) with the feature from Table 1 it corresponds to.

deformed, the persistence diagram changes continuously as well due to its stability property, and thus we see continuous curves in $\mathrm{Dgm}_0(f_4)$.

Different densities. Figure 6 shows $\mathrm{Dgm}_0(f_4)$ for experimental packings of various packing densities. Note that due to the high total number of spheres and thus persistence points, the diagram is visualized as a heatmap, each pixel representing the number of persistence points in its value range. In these experimental packings, we see points in the locations from Table 1 characteristic of FCC and HCP structures, indicating the presence of these geometric configuration in our packings. We furthermore see points along the deformation curves from Figure 5, suggesting that these deformed configurations are present at various stages.

As the packing density increases, we see persistence points typical for FCC and HCP appearing in higher frequencies, indicating that crystalline domains appear in the packing. Exploiting these characteristic signatures in the persistence diagram, we can estimate the ratio of FCC and HCP present in a given packing.

Frequency measures. Recall from Figure 4 that the persistence points $(0.61, 0.82)$, $(0.61, 0.87)$ and $(0.71, 0.87)$ appear in ratio 1:1:1 per sphere in HCP packings, while they appear in ratio 0:2:1 in FCC packings. We can "count" the number of persistence points close to these characteristic points, to be explained in more detail later. Introducing two variables f_{HCP} and f_{FCC} to denote a

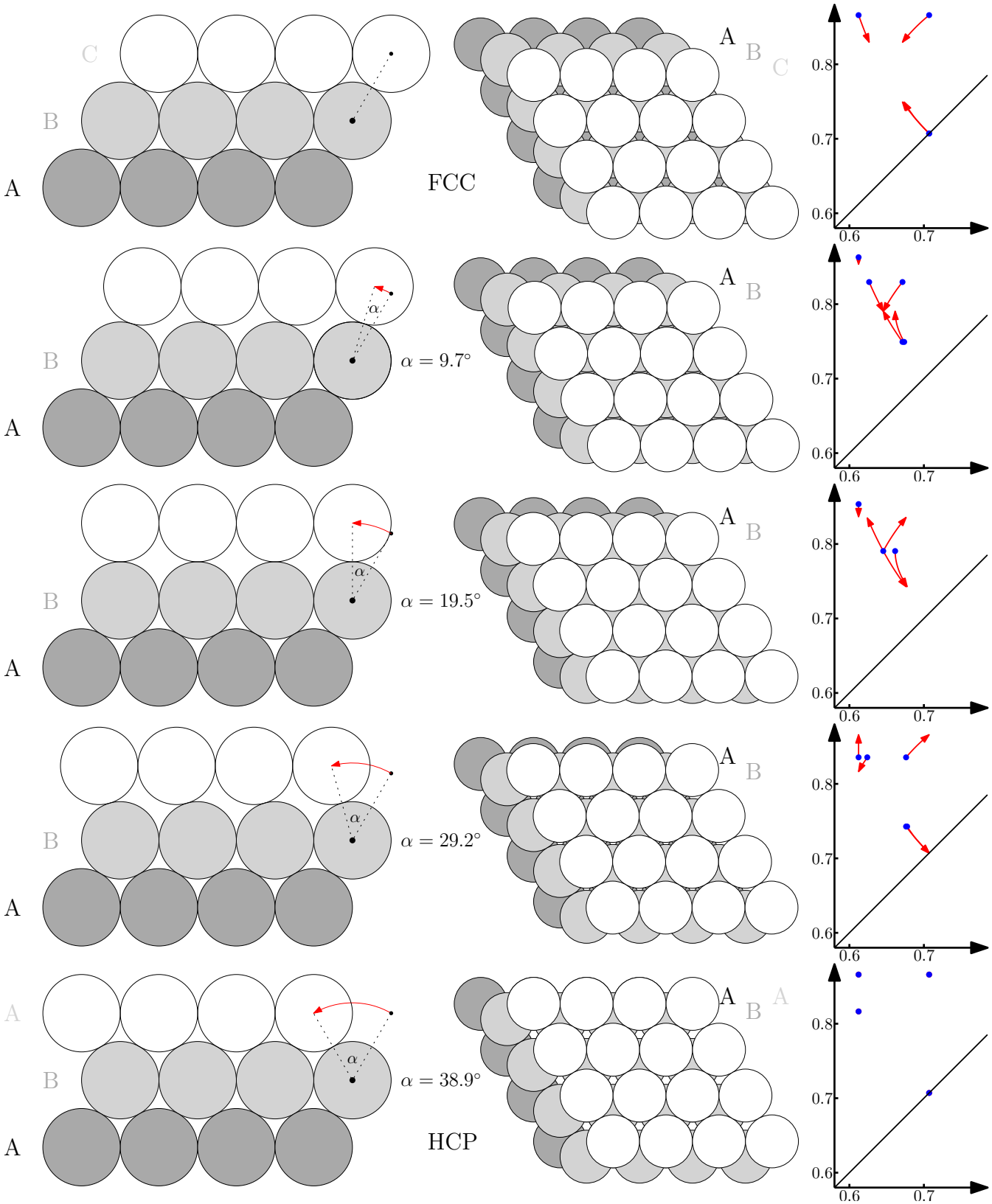

Fig. 5 Deformation of an FCC packing (first row) into an HCP packing (last row) with 3 intermediate configurations, see Supplemental Information for an animated 3D video. For each row, the first column shows a schematic sketch of the configuration with the corresponding shifting angle; the second column shows a projection from above; the third column shows the corresponding $\mathrm{Dgm}_0(f_4)$ (blue) with red curves indicating the continuous change in $\mathrm{Dgm}_0(f_4)$ when the configuration is continuously deformed into the next row's configuration.

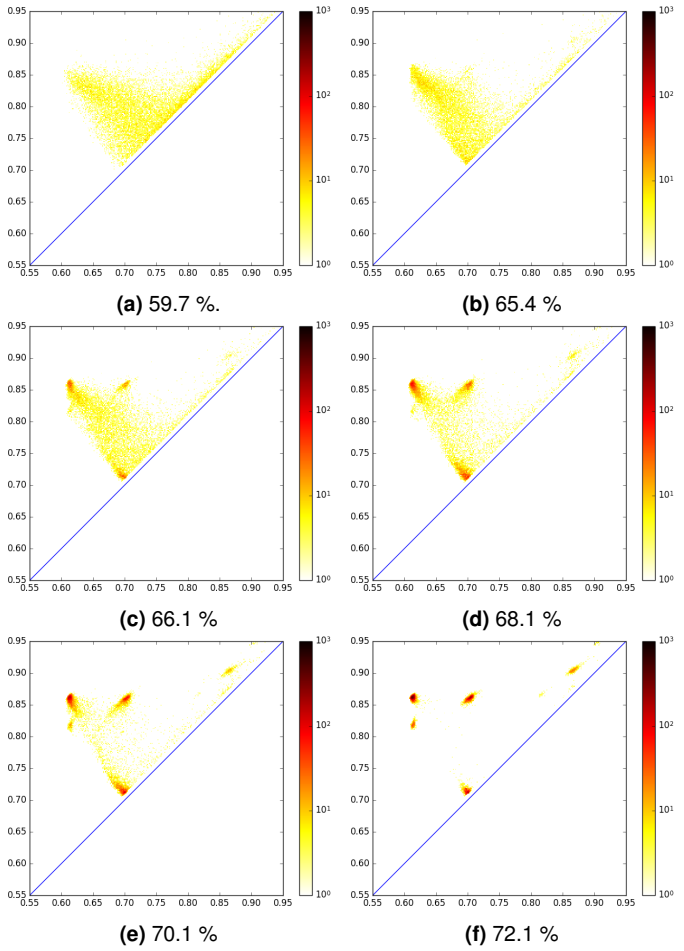

(a) 59.7 %. **(b)** 65.4 % **(c)** 66.1 % **(d)** 68.1 % **(e)** 70.1 % **(f)** 72.1 %

Fig. 6 The 4-cover persistence diagram for dimension 0, $\mathrm{Dgm}_0(f_4)$, for experimental sphere packings of various packing densities, each consisting of between 4100 and 4600 spheres.

frequency measure of HCP and FCC respectively, we find the least-squares solution to an over-defined linear system of 3 equations to estimate these frequencies of HCP and FCC and thus the ratio between HCP and FCC. The equation system is as follows:

$$\begin{aligned} f_{HCP} &= m_{face\text{-}tetra} \\ f_{HCP} + 2f_{FCC} &= m_{edge\text{-}tetra} \\ f_{HCP} + f_{FCC} &= m_{octa\text{-}tetra} \end{aligned}$$

where $m_{face\text{-}tetra}$, $m_{edge\text{-}tetra}$ and $m_{octa\text{-}tetra}$ denotes the number of persistence points "close" to $(0.61, 0.82)$, $(0.61, 0.87)$ and $(0.71, 0.87)$ respectively. Instead of directly counting how many persistence points are within a certain radius of each of these features, we rather weigh the contributions such that closer points contribute more to the count. Specifically, for each point we compute the distance between the point and the feature, and weigh it according to a Gaussian probability density function $g_\sigma(x)$ that is normalized such that $g_\sigma(0) = 1$, so that points that coincide exactly with the feature contribute 1. As standard deviation for the Gaussian we choose $\sigma = 0.005$, so that points within distance 0.005 still contribute approximately 0.6 to the count, while points at distance greater than 0.015 contribute less than 0.01. In particular, with this choice we ensure not to capture points belonging to other features, as the two closest features have a distance of approximately 0.05. For the distance, we use L_∞-distance which is the standard distance used in persistence diagrams. This choice of counting points ensures that the stability property of persistence diagrams translates to stability of our measure, meaning that small changes in the sphere packings imply small changes in estimated HCP and FCC frequency.

Figure 7 shows the values of our measure for HCP and FCC frequency as well as their ratio for different packing densities. Each data point is for an experimental packing of approximately 4000 spheres. We see similar results as observed using previous measures [11], in particular that FCC occurs more frequently in more crystalline packings than HCP.

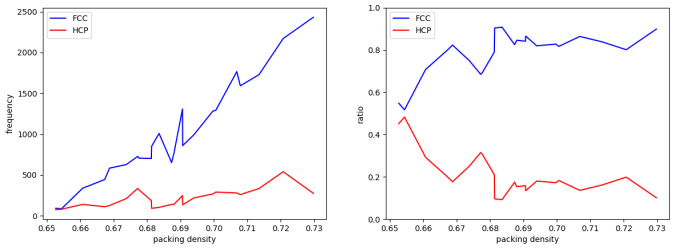

(a) Frequency of FCC and HCP. **(b)** Relative ratio of FCC and HCP.

Fig. 7 Frequency measure of HCP- and FCC-like structures as well as ratio of the two in experimental packings of different densities, according to our measure.

Notice that our method will also distinguish more complex Barlow stackings, as long as the ratios between FCC-type layer groups (i.e. 3 consecutive distinct layers, ABC) and HCP-type layer groups (i.e. 3 consecutive layers with the first and third coinciding, ABA) in the stackings are different. For example, Sm or Mo_2S_3 with ABABCBCAC stacking [12,13], Ti_4S_5 with ABABCBABAC stacking and Fe_3S_4 with ABCBCABABCAC stacking [13,14] have ratios between FCC-type and HCP-type layer groups of 2:1, 3:2 and 1:1 respectively, and thus they exhibit different $\mathrm{Dgm}_0(f_4)$ and our measure would indicate these different FCC/HCP ratios. For Barlow stackings with the same ratios, we expect $\mathrm{Dgm}_0(f_k)$ for sufficiently large k to differ.

4 Stability of FCC and HCP

As seen in Figure 7, HCP structures appear less commonly in experimental packings than FCC structures. We investigate this phenomenon using a shearing simulation in which perfectly crystalline FCC and HCP layers of frictional grains are sheared until the packing becomes disordered; see Supplemental Information for details on the simulation. This molecular dynamics simulation allows us to dynamically track the "melting" of a granular crystal from FCC/HCP to disorder. Using the 4-cover persistence diagrams, we analyse the stability of HCP and FCC patterns from a topological perspective as these motifs progress from order towards disorder. Figure 8 show the temporal evolution of $\mathrm{Dgm}_0(f_4)$ of the FCC and HCP packings as they become more and more disordered. The signature of this quasi-static transition in the topological space is highly similar to the one measured in partially crystallized packings at mechanical equilibrium.

Figure 8 compares the melting of FCC and HCP at corresponding time steps. While both structures exhibit deformation patterns similar to the ones shown in Figure 5, they are much more pronounced in the HCP melting. While the FCC packing stays stable in its (slightly perturbed) crystalline pattern, the HCP packing deteriorates into a disordered packing looking similar to Figure 6a. The birth and death coordinates of the FCC/HCP typical features are lower than they theoretically should be as shown in Figure 4, and they slightly decrease over time in the simulation. However this phenomenon is just a side effect of the simulation allowing slight overlap of spheres under strong forces.

5 Conclusions

Structures consisting of close-packed layers of hexagonally arranged spheres form the highest packing density in mono-sized sphere packing [15]. These layers can be stacked in various periodic or random fashions commonly known as "Barlow stacking". In the simplest periodic structures, the layers are arranged as ABAB..., which corresponds to the hexagonally close-packed (HCP) structure and ABCABC... for face-centered cubic (FCC) structure [16,17]. More complex examples can be found in lattice structure of metal compounds where the anions are arranged in a Barlow stacking, with the cations occupying the holes of HCP packing. [13,14].

Due to the abundance and importance of such motifs in physical systems, many techniques have been invented for their quantification, each with strengths and shortcomings. For instance the Bond Orientational Order [14,18], which is widely used in condensed matter physics to characterise local crystalline structures is a Short Range Order parameter and dependant on the choice of neighbours and it suffers from ambiguous neighbourhood definition [19] and discontinuity of neighbourhood shells [20] .

This paper presents an efficient way based on k-fold cover to unambiguously distinguish between FCC, HCP and various Barlow stacking by analysing dimension 0 of the 4-cover persistence diagram. Our approach addresses the shortcoming of [4] and unlike the Bond Orientational Orders, it is built on a continuous distance function.

Numerous studies have shown that in hard-sphere packing [17,21,22] and strongly charged colloids [23], FCC is the preferred structure despite the fact that both the FCC and HCP structures have an identical packing density of $\approx 74\%$. By tracking the 4-cover topological signatures of both FCC and HCP during the melting process, we were able to show that the FCC has a more stable structure compared with HCP.

Our results provide an opportunity to improve our understanding of non-equilibrium physics with applications including glass, granular and colloidal jamming and ordered-disordered transitions, crystal melting and nucleation [24–26]. Further, the approach presented here may have practical applications in domains such as pore description in soil- and geo-sciences [27], which are crucial for understanding natural systems and their mechanical stability, flow properties etc. [28].

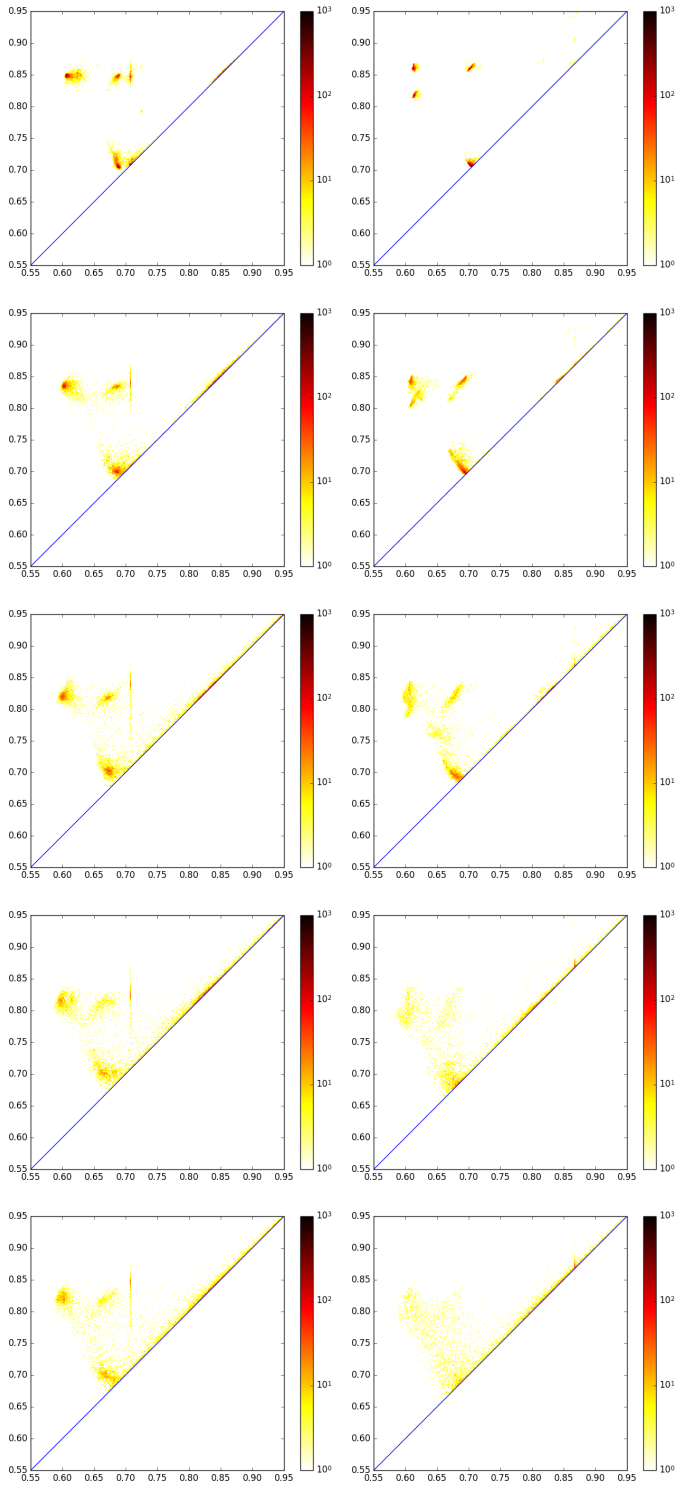

Fig. 8 4-cover $\mathrm{Dgm}_0(f_4)$ for simulated shearing of FCC (left) and HCP (right) packings at time steps 3, 11, 21, 33 and 49 of the simulation.

Conflicts of interest

The authors declare no competing interests.

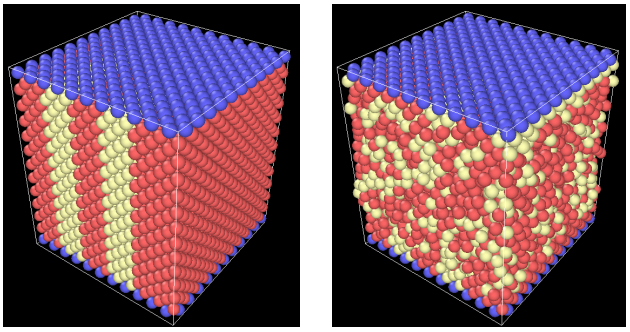

Fig. 9 Molecular Dynamics (MD) simulations of the melting process from a regular FCC lattice (left) to a disordered system (right) by inducing shear via moving the top layer grains. See Supplemental Information for a video of the simulation.

Acknowledgements

MS acknowledges the support by Australian Research Council funding through the ARC Training Centre for M3D Innovation (IC180100008). MS thanks M. Hanifpour and N. Francois for their input and valuable discussions. This project has received funding from the European Research Council (ERC) under the European Union's Horizon 2020 research and innovation programme, grant no. 788183 and from the Wittgenstein Prize, Austrian Science Fund (FWF), grant no. Z 342-N31.

A Supplemental Information

A.1 Melting of FCC and HCP: order-disorder simulations

Packings of 6,000 mono-disperse spheres are formed according to face-centred-cubic (FCC) and hexagonal-close-packing (HCP) motif. The bottom layer of grains is then set into motion at a constant shear rate. The forces (both normal and frictional) between the grains and grain displacement are computed at each time step by a discrete element method that uses Hertz–Mindlin contact model[29]. During the crystal "melting", a characteristic shear rate is evaluated as $\dot{\gamma} = v_g/(4d)$, where v_g is the velocity of shearing boundary. The simulated process is quasi-static in the sense that the characteristic time of decrease of φ is more than 10 times larger than the characteristic time associated with the shear deformation applied. During the melting, the packing remains dense with a packing density that stays larger than $\varphi = 0.54$ during the transition. Moreover, a high number of mechanical contacts is maintained throughout the process: the average mechanical coordination number Z is initially 12 and remains > 4 during the evolution.

A.2 Geometric features in FCC and HCP

We give geometric explanations for the features in Table 1. With each tetrahedral cavity, a component of the 4-fold cover emerges at radius $\sqrt{6}/4$, which is the circumradius of such a tetrahedron. The radius for which this component merges with other components depends on the neighbourhood of this tetrahedron. If it is face-adjacent, as present in the HCP packing, then it merges with that tetrahedron's component at radius $\sqrt{6}/3$, which is the height of a tetrahedron or equivalently the radius when a ball centered around one of the tetrahedral vertices touches the opposite face. This explains the point $(\sqrt{6}/4, \sqrt{6}/3)$ in the persistence diagram of the HCP packing. If instead another tetrahedron is adjacent via an edge at the angle like in FCC and HCP, their components only merge at radius $\sqrt{3}/2$, which is the distance from a tetrahedral vertex to any of its opposite edges, equaling the height of a triangular face. This explains the point $(\sqrt{6}/4, \sqrt{3}/2)$ in the persistence diagram. In FCC packings this configuration is twice as frequent as in HCP packings, and thus appears with multiplicity 2 there. Finally, both configurations contain octahedra that share faces with tetrahedra. The circumradius of an octahedron is $\sqrt{2}/2$. Thus within octahedra, the 4-fold cover only emerges at radius $\sqrt{2}/2$ at the circumcenter of the octahedron. It merges with the component of a face-adjacent tetrahedron at radius $\sqrt{3}/2$, which is half the distance between the vertex unique to the tetrahedron (i.e. not shared with the octahedron) to any of the vertices unique to the octahedron (i.e. not shared with the tetrahedron). This distance equals the height of a regular triangle, $\sqrt{3}/2$, as each of the non-shared tetrahedral faces is co-planar with the incident octahedral face. This explains the persistence point at $(\sqrt{2}/2, \sqrt{3}/2)$. As there are 6 rather than merely 4 points at the same distance from the circumcenter of an octahedron, when the octahedron is slightly deformed it is possible that multiple components arise at a radius close to $\sqrt{2}/2$ which merge together very quickly. So while in a perfect packing these components have 0-persistence, in experimental packings we will often also see persistence points close to the diagonal at $(\sqrt{2}/2, \sqrt{2}/2)$, stemming from this phenomenon. These are present whenever octahedra are present, and thus appear in both slightly deformed FCC and HCP packings.

Notes and references

1 J. D. Bernal, *Nature*, 1959, **183**, 141 – 147.

2 T. Aste, M. Saadatfar and T. J. Senden, *Phys. Rev. E*, 2005, **71**, 061302.

3 M. Jerkins, M. Schröter, H. L. Swinney, T. J. Senden, M. Saadatfar and T. Aste, *Phys. Rev. Lett.*, 2008, **101**, 018301.

4 M. Saadatfar, H. Takeuchi, V. Robins, N. Francois and Y. Hiraoka, *Nature communications*, 2017, **8**, 1–11.

5 F. Rietz, C. Radin, H. L. Swinney and M. Schröter, *Physical review letters*, 2018, **120**, 055701.

6 V. Robins and K. Turner, *Physica D: Nonlinear Phenomena*, 2016, **334**, 99–117.

7 H. Edelsbrunner and J. Harer, *Computational Topology. An Introduction*, American Mathematical Society, Providence, RI, 2010.

8 H. Edelsbrunner, D. Letscher and A. Zomorodian, Proceedings 41st Annual Symposium on Foundations of Computer Science, 2000, pp. 454–463.

9 D. Cohen-Steiner, H. Edelsbrunner and J. Harer, Proceedings of the Twenty-First Annual Symposium on Computational Ge-

ometry, New York, NY, USA, 2005, pp. 263–271.
10 H. Edelsbrunner and G. Osang, 34th International Symposium on Computational Geometry (SoCG 2018), 2018, p. 34.
11 M. Hanifpour, N. Francois, V. Robins, A. Kingston, S. M. Vaez Allaei and M. Saadatfar, *Phys. Rev. E*, 2015, **91**, 062202.
12 A. Overhauser, *Physical review letters*, 1984, **53**, 64.
13 A. Wells, *Structural Inorganic Chemistry. Oxford University Press*, 1984.
14 T. M. Middlemas, F. H. Stillinger and S. Torquato, *Physical Review E*, 2019, **99**, 022111.
15 T. C. Hales, *Annals of mathematics*, 2005, **162**, 1065–1185.
16 S. Heitkam, W. Drenckhan and J. Fröhlich, *Physical review letters*, 2012, **108**, 148302.
17 F. Pacheco-Vázquez, G. A. Caballero-Robledo and J. Ruiz-Suárez, *Physical review letters*, 2009, **102**, 170601.
18 B. A. Klumov, Y. Jin and H. A. Makse, *The Journal of Physical Chemistry B*, 2014, **118**, 10761–10766.
19 M. Hanifpour, N. Francois, S. V. Allaei, T. Senden and M. Saadatfar, *Physical review letters*, 2014, **113**, 148001.
20 W. Mickel, S. C. Kapfer, G. E. Schröder-Turk and K. Mecke, *The Journal of Chemical Physics*, 2013, **138**, 044501.
21 A. Van der Net, W. Drenckhan, D. Weaire and S. Hutzler, *Soft Matter*, 2006, **2**, 129–134.
22 N. Francois, M. Saadatfar, R. Cruikshank and A. Sheppard, *Physical review letters*, 2013, **111**, 148001.
23 J. Hoogenboom, A. Yethiraj, A. van Langen-Suurling, J. Romijn and A. Van Blaaderen, *Physical review letters*, 2002, **89**, 256104.
24 A. Baule, F. Morone, H. J. Herrmann and H. A. Makse, *Reviews of Modern Physics*, 2018, **90**, 015006.
25 A. Panaitescu, K. A. Reddy and A. Kudrolli, *Physical review letters*, 2012, **108**, 108001.
26 A. Mughal, H. Chan, D. Weaire and S. Hutzler, *Physical Review E*, 2012, **85**, 051305.
27 A. Sufian, A. R. Russell, A. J. Whittle and M. Saadatfar, *Granular Matter*, 2015, **17**, 727–742.
28 V. Robins, M. Saadatfar, O. Delgado-Friedrichs and A. P. Sheppard, *Water Resources Research*, 2016, **52**, 315–329.
29 M. Hanifpour, N. Francois, V. Robins, A. Kingston, S. V. Allaei and M. Saadatfar, *Physical Review E*, 2015, **91**, 062202.